This is the Pre-Published Version.

The following publication Y. Li et al., "DC Fault Detection in MTDC Systems Based on Transient High Frequency of Current," in IEEE Transactions on Power Delivery, vol. 34, no. 3, pp. 950-962, June 2019 is available at https://doi.org/10.1109/TPWRD.2018.2882431.

DC Fault Detection in MTDC Systems Based on Transient High-frequency of Current

Yujun Li, Lei Wu, Jiapeng Li, Liansong Xiong, *Member, IEEE*, Guobing Song, *Member, IEEE*, Zhao Xu, *Senior Member, IEEE*

***Abstract*—Isolation of the fault DC lines during initial short period after fault is a major challenge in the multi-terminal DC (MTDC) system based on voltage source converter (VSC). Existing protection schemes are mainly designed based on the numerical simulations, which lacks of the theoretical analysis. In this paper, a high-frequency equivalent model of VSC based MTDC system is firstly proposed for the fault current calculation. Based on the DC fault analysis, it is validated that high-frequency fault current components flow in the fault line and then dramatically decay in the healthy line. Accordingly, a novel DC fault detection method for VSC based MTDC system is proposed. In the proposed approach, the primary protection utilizes the transient high-frequency energy of line current and the fault line can be identified quickly without communication. In addition, the influence of the transient traveling-wave appearing on the long-transmission line on the proposed protection scheme is also investigated. Numerous simulation studies carried out in PSCAD/EMTDC have demonstrated that the proposed high-frequency equivalent model can be utilized for initial DC fault analysis of VSC based MTDC system and the proposed protection scheme is effective in different time windows, different fault locations and high fault resistances. Compared with the existing rate of change of current (ROCOC) based protection scheme, the proposed primary protection requires relatively low sampling frequency, is insensitive to the parameter changes, and has high robustness with respect to the outside noises and data missing.**

***Index Terms*—Fault analysis, high frequency equivalent model, VSC based MTDC, transient high-frequency current.**

I. Introduction

RECENTLY, the voltage source converter (VSC) based high voltage direct current (HVDC) system has been widely utilized in variable industrial application such as integration of large amount of renewable energy and interconnection of asynchronous network [1]. A multi-terminal DC grid (MTDC) system contains multiple converters interconnected with DC lines in meshes or radials [2], and it is considered as one of the best solutions for connecting large-scale of fluctuating renewables over long distances. One such project currently under envisaged and proposed is European "Super Grid" [3] that utilizes MTDC grid to connect large-scale offshore wind farms with the European mainland. A major challenge for future development of DC grid is fault analysis and fault detection in a mesh MTDC grid [4-18].

A. Related works

Short-circuit current calculation is very necessary and crucial for the power system and protection design. For the fault current calculation of MTDC system, [4] and [5] deduced the analytical equation for single terminal HVDC system, which is not suitable for the fault current calculation in the multi-terminal system since the mutual coupling of each converter should be considered in the fault analysis. References [6] and [7] presents the DC fault analysis of two-level VSC and MMC based MTDC system. However, the results are mainly based on the electromagnetic transient (EMT) simulations, which is quite time-consuming when the DC network is large and complex. In addition, the simulations can only provide the information by several scenarios. A generic fault current calculation algorithm for DC grid is proposed in [8] that establishes the fault matrix of the entire DC grid. However, this method can not give the clear analytical expression of the fault current nor the parameters that influence the fault current.

Understanding the fault characteristic of DC grid is vital for designing effective DC fault detection methods. Current differential method [9] is an ideal way to achieve fault detection with high selectivity. However, it requires the information from both sides of the transmission line end, and the enough consecutive samples are needed for the relay setting. The communication delay due to the long transmission line may not suitable for the fast primary protection in a DC grid. In order to improve DC fault detection performance, transient components are widely utilized for the protection design [10]. Using transient harmonic current that depends on a single-frequency component for two-terminal HVDC system is proposed in [11, 12]. However, this method is vulnerable to be disturbed by noises, and may not suitable for multi-terminal HVDC system since multi resonance frequencies exist in the system. Another method that achieves fast fault detection is employing the travelling-wave based method by detecting the voltage derivative and current derivative [13, 14]. However, this method requires high-frequency sampling and is sensitive to the fault resistance.

The DC reactors [15] connected at the end of each DC line are utilized for limiting the DC fault current, and can be regarded as a useful means for fast DC protection. Reference [16] uses the rate of change of the voltage measured across the

This work was supported in part, in part by the National Natural Science Foundation of China under Grants 51807150, 51707091, and U1766209, in part by the China Postdoctoral Science Foundation (2018M640989), and in part by "the Fundamental Research Funds for the Central Universities" (xjj2018006).

Y. Li is with the School of Electrical Engineering, Xi'an Jiaotong University. He is also with the Department of Electrical Engineering, The Hong Kong Polytechnic University, Hong Kong (email: yujunlizju@gmail.com).

L. Wu, J. Li and G. Song is with the School of Electrical Engineering, Xi'an Jiaotong University (email: barry_wui@163.com, wennuanfrank@gmail.com, song.gb@163.com).

L. Xiong is with the School of Automation, Nanjing Institute of Technology. He is also with the Department of Electrical Engineering, The Hong Kong Polytechnic University, Hong Kong (email: xiongliansong@163.com).

Z. Xu are with the Department of Electrical Engineering, The Hong Kong Polytechnic University, Hong Kong (email: eezhaoxu@polyu.edu.hk).

© 2018 IEEE. Personal use of this material is permitted. Permission from IEEE must be obtained for all other uses, in any current or future media, including reprinting/republishing this material for advertising or promotional purposes, creating new collective works, for resale or redistribution to servers or lists, or reuse of any copyrighted component of this work in other works.

DC reactor, and [17] utilizes the DC reactor voltage for identifying the fault line in 2 ms or less. Reference [18] uses high-frequency components of DC reactor voltage by calculating the ratio of the transient voltages at both side of inductor. Existing methods [16-18] are mainly based on detecting the transient components on the DC reactors at the end of each lines, which add new measurement equipment and lower the reliability of the protection. In addition, the appropriate frequency band is not provided in [18].

Existing rate of change of current or voltage (ROCOC or ROCOV) method and travelling-wave method normally requires extremely high-sampling frequency (hundreds of kHz or 1MHz) so that the first reflection of the current/voltage travelling-wave can be captured. However, in the practical engineering, the primary protection relay will be activated by detecting three or four continuous ROCOC or ROCOV that are over the set threshold. As a result, the traditional methods are vulnerably invalid when the sampling frequency is relatively low, or missing the first few data of initial DC fault current.

B. *Main contribution*

Most existing literatures focus on the fault analysis of MTDC system based on the numerical simulations and complex fault matrix, resulting in the fault current analytical expression not clearly presented. However, the primary protection of MTDC system concerns on the initial short period after fault. Therefore, this paper firstly proposes a simplified high-frequency equivalent model of MTDC grid for fault current calculation.

A novel DC fault detection method for VSC based MTDC system is further proposed. It is validated that high-frequency fault current components of fault line are larger than that in the healthy line. Accordingly, the primary detection utilizes the transient high-frequency energy of line current and the fault line can be identified quickly using one-end information. The influence of the transient traveling-wave appearing in the long-transmission line on the proposed protection scheme is also investigated. Compared with the traditional protection schemes based on ROCOC, the proposed one stands out for relatively low sampling frequency, insensitive to the parameter changes, and high robustness with respect to the outside noises and data missing. Simulation studies have demonstrated that the proposed protection scheme is effective in different time windows, different fault locations and high fault resistances.

II. DC Fault Current Calculation in MTDC System

A. *Typical topology of MTDC system*

In a meshed DC grid, fault DC line should be accurately identified in several milliseconds for DC circuit breaker (CB) to operate after a DC short-circuit fault. When a pole-to-ground DC fault occurs, the parallel connected capacitors of VSC begin to discharge and the fault current surges dramatically. Meanwhile, during the initial short period after fault, the VSC can still be regarded as a current-controlled source due to the small drop of DC-link voltage, and the fault component from ac side source can be ignored for fault analysis during short-time period. Accordingly, the VSC can be simply regarded as parallel connected capacitors for DC fault analysis.

A typical three-terminal DC grid that incorporates a solid pole-to-ground DC fault at the Line 12 is shown in Fig. 1. The supplemental inductor at DC side is usually implemented to reduce the DC current ripple, as the same effect as the smoothing reactor in the LCC-based HVDC. Recently, in order to limit the peak value and the rising rate of the DC fault current, large inductor with several hundreds of mH is applied in MTDC system so that DC CB can interrupt the fault current in several milliseconds. In order to facilitate the analysis, the DC overhead lines are approximated as series RL circuits, the influence of the travelling-wave during transient process will be further discussed in the Section IV. R_{mk} and L_{mk} are the resistance and inductance of the Line *mk*. R_{m0} and L_{m0} are the resistance and inductance to the fault location from side *m*. L_{Tmk} is the DC supplemental inductor at the *m* side of branch *mk*. C_{cm} is the DC-link capacitance of VSC*m*.

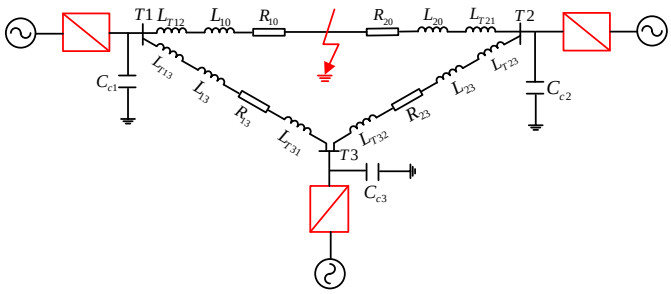

Fig. 1. RLC circuit of the typical three-terminal DC grid

B. *Calculation of short-circuit DC current*

It is noted that the steady-state component can be negligible compared to the fault current component. Accordingly, the steady-state DC current has little high-frequency component. Therefore, only fault component of DC line current is considered. According to the superposition principle, the fault component of DC current can be calculated by solving the passive network with only one voltage source U_0. In order to facilitate the analysis, the positive direction of DC line current is defined from healthy line to the fault line. When calculating the fault current component, *Laplace Transformation* method is widely utilized since the fault current calculation is converted to the algebraic operation instead of complex derivation operation. Laplace circuit should be firstly formulated for calculating the fault component of each branch line, and there is only one Laplace circuit for calculating the responses of multiple frequencies generated from the fault location.

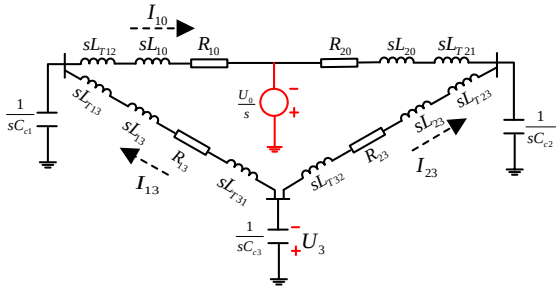

Fig. 2. Laplace circuit of the studied three-terminal DC network for calculating the fault component.

Fig. 2 shows the Laplace circuit of the studied three-terminal DC network for calculating fault current component. The DC-link capacitor voltage of Terminal 3 can be expressed as follows:

$$U_3(s) = (I_{13}(s) + I_{23}(s)) \cdot \frac{1}{sC_{c3}} \tag{1}$$

where U_3 is the DC-link capacitor voltage of the Terminal 3. I_{13}, I_{23} are the DC line current of Line 13 and 23, respectively. In order to facilitate the calculation, the DC-link capacitor branch of Terminal 3 can be decoupled into two independent capacitors, which belong to Line 13 and 23. The corresponding impedance should be satisfied as follows,

$$\begin{cases} Z_{c13}(s) = \dfrac{(I_{13}(s) + I_{23}(s)) \cdot \dfrac{1}{sC_{c3}}}{I_{13}(s)} \\ Z_{c23}(s) = \dfrac{(I_{13}(s) + I_{23}(s)) \cdot \dfrac{1}{sC_{c3}}}{I_{23}(s)} \end{cases} \tag{2}$$

where, Z_{c13}, Z_{c23} are the impedance of two decoupled capacitors, which belong to Line 13 and 23 respectively. Define the proportional coefficient of DC current of Line 13 and Line 23 as follows:

$$k = I_{23}(s) / I_{13}(s) \tag{3}$$

where, k is correlated proportional coefficient and it is related with the fault location of the Line 12, the length of the transmission Line 23 and 13, and the inductance of the supplementary inductor. If the circuit as shown in Fig. 2 is symmetrical, then k=1. The capacitance of two independent capacitors marked as C_{c13} and C_{c23}, which belong to Line 13 and 23 can be expressed as follows,

$$\begin{cases} C_{c13} = \dfrac{C_{c3}}{1+k} \\ C_{c23} = \dfrac{C_{c3}}{1+1/k} \end{cases} \tag{4}$$

Accordingly, the meshed MTDC system can be unlocked into two independent radical networks shown in Fig. 3. Therefore, the fault current component of the fault line I_{10} can be expressed as follows,

$$\begin{aligned} I_{10}(s) &= \frac{U_0 / s}{R_{10} + s(L_{10} + L_{T12}) + Z_{f10}(s)} \\ Z_{f10}(s) &= 1/sC_{c1} \cdot \frac{s(L_{13} + L_{T13} + L_{T31}) + 1/sC_{c13} + R_{13}}{s(L_{13} + L_{T13} + L_{T31}) + 1/sC_{c1} + 1/sC_{c13} + R_{13}} \end{aligned} \tag{5}$$

where, Z_{f10} is total impedance of the DC-link capacitor of Terminal 1 parallel connected with branch Line 13.

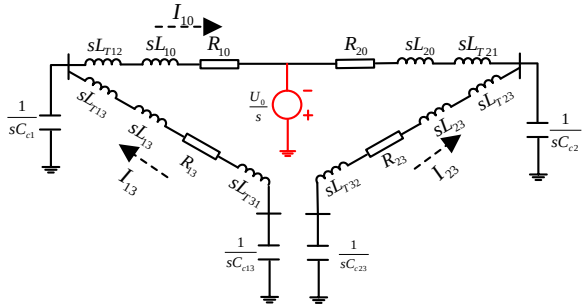

Fig. 3. Unlock meshed MTDC system into two independent radical networks.

C. High frequency equivalent model

It is very difficult to get the mathematic expression of $I_{10}(t)$ based on the *Inverse Laplace Transform* of (5). Therefore, an equivalent model should be put forward to obtain an approximate expression of $I_{10}(t)$ during the initial short period after fault. Considering *Discrete Fourier Transform* (DFT) of fault line DC current, it yields as follows,

$$X(k) = \sum_{n=0}^{N-1} I_{10}(n) \cdot e^{-j\frac{2\pi}{N}kn} \tag{6}$$

where $X(k)$ is the DFT of the transient fault line current. N is the number of samples in a period of T. Rewrite (6) in a continuous form, which is given by:

$$X'(k) = \frac{X(k)}{N} = \frac{1}{N}\sum_{n=0}^{N-1} I_{10}(n) \cdot e^{-j\frac{2\pi}{N}kn} \approx \frac{1}{T}\int_0^T I_{10}(t) \cdot e^{-j\frac{2\pi}{T}kt} \cdot dt \tag{7}$$

where $X'(k)$ is the *Discrete Fourier Series* of (5). In order to deduce the high-frequency equivalent model, two ***Lemmas*** should be introduced as follows:

Lemma 1: DFT of the continuous aperiodic signal $f(t)$ equals to the $-j\omega N$ multiple the *Fourier Transform* of $f(t)$ on the condition that the sampling time is short enough.

Proof: The general format of *Continuous Fourier Series* can be written as follows,

$$G(\omega, T) = \frac{1}{T}\int_0^T f(t) \cdot e^{-j\omega t} \cdot dt \tag{8}$$

Considering small sampling time of T and $f(0)$=0, $f(t)$ can be expressed as follows by using *Taylor Series* around zero,

$$f(t) = f(0) + f'(0) \cdot t + f''(0)/2 \cdot t^2 + \ldots\ldots \approx f'(0) \cdot t \tag{9}$$

Combining (8) and (9), the following expression can be hold,

$$G(\omega, T) \approx \frac{1}{T} \cdot \int_0^T f'(0) \cdot t \cdot e^{-j\omega t} \cdot dt = -\frac{f'(0)}{j\omega} \tag{10}$$

Considering the classical *Fourier Transform* of $f(t)$,

$$F(\omega) = \int_0^\infty f(t) \cdot e^{-j\omega t} \cdot dt \approx \int_0^\infty f'(0) \cdot t \cdot e^{-j\omega t} \cdot dt = \frac{f'(0)}{(j\omega)^2} \tag{11}$$

Based on (10) and (11), the following expression can be obtained,

$$\left|G(\omega, T)\right| \approx \left|-j\omega \cdot F(\omega)\right| = \frac{f'(0)}{\omega} \tag{12}$$

Rewrite (12) in a *Laplace form* and based on (7),

$$\left|DFT(f(t))\right| = N \cdot \left|s \cdot L(f(t))\right|_{s=k\cdot\frac{2\pi}{N}f_s \cdot j} \tag{13}$$

END

Lemma 2: The continuous aperiodic signal $f(t)$ equals to the *Inverse Laplace Transform* of high-frequency part of the *Laplace Transform* of $f(t)$ during initial period of the signal.

Proof: Suppose $X(k)$ is the DFT of the aperiodic signal $f(t)$, the following expression should be hold as follows:

$$\left|X(k)\right| = \left|DFT(f(t))\right| \approx N \cdot \left|s \cdot L(f(t))\right|_{s=k\cdot\frac{2\pi}{N}f_s \cdot j} \tag{14}$$

where, f_s is the sampling frequency. The frequency interval of DFT of the signal $X(k)$ marked as Δf can be expressed as follows,

$$\Delta f = \frac{1}{N} f_s = \frac{1}{T} \tag{15}$$

When the sampling cycle T is small, the frequency interval of the DFT will be large enough, and DFT of the aperiodic signal $f(t)$ is approximately as follows,

$$\left|X(k)\right| = N \cdot \left|s \cdot L(f(t))\right|_{s=k\cdot\frac{2\pi}{N}f_s\cdot j} \approx N \cdot \left|s \cdot L^H(f(t))\right|_{s=k\cdot\frac{2\pi}{N}f_s\cdot j} \tag{16}$$

where, $L^H(f(t))$ is the high-frequency component of *Laplace Transform* of the signal $f(t)$. Define another continuous aperiodic signal $g(t)$, which can be expressed as follows,

$$g(t) = L^{-1}(L^H(s)) \tag{17}$$

The DFT of the aperiodic signal $g(t)$ should satisfy below,

$$\left|DFT(g(t))\right| = N \cdot \left|s \cdot L^H(f(t))\right|_{s=k\cdot\frac{2\pi}{N}f_s\cdot j} \approx DFT(f(t)) \tag{18}$$

Based on (17) and (18), the following expression is hold,

$$f(t) \approx g(t) = L^{-1}(L^H(s)) \tag{19}$$

END

This ***Lemma*** implies when analyzing the initial period of the signal, the initial expression of the *f(t)* equals to *Inverse Laplace Transform* of high-frequency part of the *Laplace Transform* of *f(t)*. This ***Lemma*** gives an important guidance for the model simplification if the initial stage of signal is more concerned for the system operator. Based on the above ***Lemma* 2**, in the high-frequency region, Z_{f10} in (5) can be regarded as only a DC-link capacitor for fault analysis, which is written as follows,

$$Z_{f10}{}^H(s) \approx 1/sC_{c1} \tag{20}$$

Correspondingly, the high-frequency part of *Laplace Transform* of DC fault line current can be written as follows,

$$I_{10}{}^H(s) = \frac{U_0/s}{R_{10} + s(L_{10} + L_{T12}) + 1/sC_{c1}} \tag{21}$$

Similarly, the fault current component of healthy line I_{13} can be written as follows,

$$I_{13}(s) = I_{10}(s) \cdot \frac{1/sC_{c1}}{s(L_{13} + L_{T13} + L_{T31}) + 1/sC_{c13} + 1/sC_{c1} + R_{13}} \tag{22}$$

Then, the high-frequency part of *Laplace Transform* of DC healthy line current can be written as follows,

$$\begin{cases} I_{13}{}^H(s) = I_{10}{}^H(s) \cdot h(s) \\ h(s) = \dfrac{1}{s^2(L_{13} + L_{T13} + L_{T31})C_{c1} + (1+k)C_{c1}/C_{c3} + sR_{13}C_{c1} + 1} \end{cases} \tag{23}$$

The (21) and (23) indicates the high-frequency equivalent model of three-terminal MTDC grid. Based on (21) and (23), the fault current component of healthy line equals to that of the fault line multiple $h(s)$. The transfer function $h(s)$ has the same characteristic of the second-order low-pass filter. Therefore, the high-frequency fault current components of healthy line decay largely compared to that of the fault line.

The objective of the paper is to calculate the initial DC fault current, which is corresponding to the proposed high-frequency equivalent model. The influence of the correlated proportional coefficient (k) on the fault current calculation is very limited since the two independent capacitors marked as C_{c13} and C_{c23} of VSC can be negligible in the high-frequency zone. In addition, with the increase of the DC terminals (such as four or five terminal DC grid, the DC lines that are far away from the fault line can be regarded as constant current-source during initial period of the fault. The meshed MTDC network is automatically decoupled by two independent circuits, and k will be equal to 0.

The above analysis is applied to a three-terminal DC grid. For a general MTDC system, when overlooking the influence of the correlated proportional coefficient (k) on the fault current calculation, the generic formula of $h(s)$ can be expressed as follows,

$$h_n(s) = \frac{1}{s^2(L_{ij} + L_{Tij} + L_{Tij})C_{c1} + C_{ci}/C_{cj} + sR_{ij}C_{ci} + 1} \tag{24}$$

where, n is the subscript of the $h_n(s)$, and it describes the *Line level* of the health line. For instance, if one health line directly connects to the fault line, then the *Line level* marks as 1. If another health line connects to the *Level* 1 health line, then the *Line level* will be 2. In the high-frequency region, the $h_n(s)$ can be further deduces as (25),

$$\begin{aligned} h_n(s) &= \frac{1}{s^2(L_{ij} + L_{Tij} + L_{Tij})C_{ci} + C_{ci}/C_{cj} + sR_{ij}C_{ci} + 1} \\ &\approx \frac{1}{s^2(L_{ij} + L_{Tij} + L_{Tij})C_{ci}} \end{aligned} \tag{25}$$

For a general MTDC system, the high-frequency equivalent model for the fault line and healthy line current calculation is written below,

$$\begin{cases} I_{10}{}^H(s) = \dfrac{U_0/s}{R_{10} + s(L_{10} + L_{T12}) + 1/sC_{c1}} \\ I_{ij}{}^H(s) = I_{10}{}^H(s) \cdot \prod_{n=1}^{m} h_n(s) \end{cases} \tag{26}$$

The fault current component of healthy line *ij* equals to that of upper level line multiple a second-order low-pass filter $h_n(s)$.

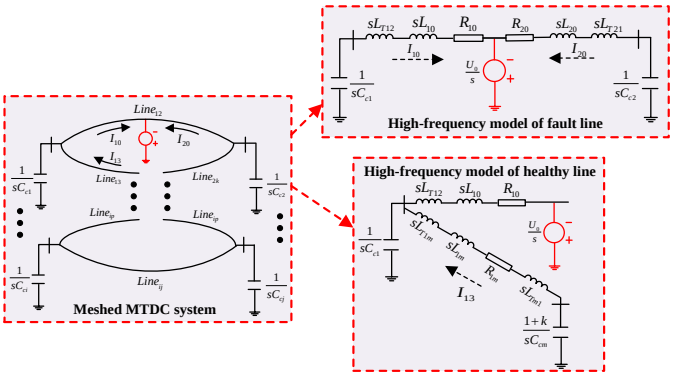

Fig. 4. high-frequency model of meshed MTDC system for fault current calculation.

D. Determination of the cut-off frequency

Apparently, it can be seen that high-frequency fault current components dramatically decay in the healthy line due to the low-pass filter characteristic of $h(s)$. Therefore, it is crucial to determine a cut-off frequency that can distinctively identify the fault line. Rewrite $h(s)$ in (23), and assume $C_{c1} = C_{c3}$,

$$\begin{aligned} h(s) &= \frac{1/\tau}{s^2 + sR_{13}C_{c1}/\tau + (2+k)/\tau} \\ \tau &= (L_{13} + L_{T13} + L_{T31})C_{c1} \end{aligned} \tag{27}$$

τ in (27) is the correlated coefficient. Actually, there are many ways to define the cut-off frequency, at which frequency, the magnitude of the $h(s)$ is sufficient low so that the high-frequency fault current component of the healthy line and the fault line current can be easily identified. Define f_{oc} as the resonance frequency, and the DC-link capacitor of Terminal 1 is parallel resonated with branch Line 13 at this frequency.

$$f_{oc} = \frac{1}{2\pi} \cdot \sqrt{\frac{(2+k)}{\tau}} \tag{28}$$

In this paper, in order to get a sufficient low magnitude of the $h(s)$, the defined cut-off frequency should be above 10 times of resonance frequency defined below,

$$f_{cut} \geq 10 \cdot f_{oc} \tag{29}$$

where, f_{cut} is the cut-off frequency. The magnitude of $h(s)$ should satisfy the following inequality constraints:

$$|h(s)| \leq \left| \frac{1/\tau}{(10 \cdot \sqrt{(2+k)/\tau} \cdot R_{13} C_{c1} / \tau) i - 99 \cdot (2+k)/\tau} \right| \leq \frac{1}{99 \cdot (2+k)} \tag{30}$$

It can be seen from above equation that the high-frequency fault current component ratio of fault line and healthy line is relatively high. Meanwhile, the cut-off frequency can not be too large, since the high-frequency fault current component of fault line is so small that can not be detected and can be regarded as noises or harmonics. Therefore, the following inequality constraints of cut-off frequency should be satisfied,

$$\left| X^{10}(k) \right| = \left| DFT(I_{10}(t)) \right| \geq {I_{10}}^{H}{}_{\min} \tag{31}$$

where, $X^{10}(k)$ is the DFT of the transient fault Line 10 current. ${I_{10}}^{H}{}_{\min}$ is the magnitude of minimal detectable current or the maximum harmonics value, set as 10 A in the paper. Ignoring the parallel connected capacitor of VSC in the high-frequency region, and considering that the fault happens at the end of Line 12, the fault current component of Line 12 can be written,

$${I_{10}}^{H}(s) = \frac{U_0 / s}{R_{12} + s(L_{12} + L_{T12})} \tag{32}$$

Transforming (32) into time-domain expression, based on ***Lemma* 2**, the fault line current during initial short period after fault can be roughly expressed as follows,

$$\begin{aligned} I_{10}(t) &= \left(\frac{U_0}{R_{12}} - \frac{U_0}{R_{12}} \cdot e^{-t/\tau_1}\right) \cdot \varepsilon(t) \\ \tau_1 &= (L_{12} + L_{T12}) / R_{12} \end{aligned} \tag{33}$$

where, τ_1 is the time constant of *RL* circuit, replacing $I_{10}(t)$ in (7) with (33), the *Continuous Fourier Series* of fault line current can be written in (34).

$$I_{10}(\omega) = \frac{1}{T} \int_0^T I_{10}(t) \cdot e^{-j\omega t} \cdot dt = \frac{1}{T} \cdot \frac{U_0}{R_{12}} \cdot \frac{(e^{-T/\tau_1} - 1)}{(i\omega + 1/\tau_1)} \tag{34}$$

The length of the signal T is normally around 2 ms (DC fault should be identified within 2~3 ms in a meshed MTDC sytem), and the time constant value τ_1 is around 0.1 s for metallic fault. Therefore, the expression T/τ_1 is relatively small. Using *Taylor series* around zero, the magnitude-frequency relationship of transient fault line current can be expressed as follows,

$$\left| I_{10}(\omega) \right| = \frac{U_0}{R_{12}} \cdot \frac{1}{\tau_1} \cdot \frac{1}{\sqrt{\omega^2 + 1/\tau_1^{\,2}}} \approx \frac{U_0}{\omega (L_{12} + L_{T12})} \tag{35}$$

Considering the inequality constraints of (31), the cut-off frequency should also be satisfied as follows,

$$\frac{U_0}{2\pi f_{cut} (L_{12} + L_{T12})} \geq {I_{10}}^{H}{}_{\min} \tag{36}$$

Based on (29) and (36), the cut-off frequency should be determined based on the following inequality constrains:

$$10 \cdot f_{oc} \leq f_{cut} \leq \frac{1}{2\pi} \cdot \frac{U_0}{{I_{10}}^{H}{}_{\min} \cdot (L_{12} + L_{T12})} \tag{37}$$

Based on the Nyquist–Shannon sampling theorem, the sampling frequency f_s should be satisfied as follows,

$$f_s \geq 2 f_{cut} \tag{38}$$

Therefore, the minimal sampling frequency requirement should be larger than 20 times of resonance frequency as below,

$$f_{s\min} \geq 20 \cdot f_{oc} \tag{39}$$

Resonance frequency defined in (28) is normally as 20~100 Hz, and the proposed protection scheme requires relatively low sampling frequency compared to the traditional rate of change of current or voltage (ROCOC or ROCOV) based method that high sampling frequency is necessary.

III. Primary Protection Scheme

A. Transient high-frequency energy

As previous section shows, the high-frequency fault current components flow in the fault line and then dramatically decay in the healthy line. DFT is an effective method for extraction of high-frequency components of DC line current. DFT of the transient signal can be expressed as follows,

$$X'(k) = \frac{X(k)}{N} = \frac{1}{N} \sum_{n=0}^{N-1} f(n) \cdot e^{-j\frac{2\pi}{N}kn} \tag{40}$$

where $X(k)$ is the DFT of the transient signal. $X'(k)$ is the Discrete Fourier Series. Therefore, the transient high-frequency energy of the signal at specific frequency band can be defined,

$$E = \sum_{k=i}^{k=j} \left| X'(k) \right|^2 = \frac{1}{N^2} \sum_{k=i}^{k=j} \left| X(k) \right|^2 \tag{41}$$

Accordingly, the selected frequency band in (41) is within the frequency band in (37), which can be expressed as follows,

$$\begin{aligned} i &= round\left(\frac{10 \cdot f_{oc}}{f_s / N}\right) + 1 \\ j &= round\left(\frac{1}{2\pi} \cdot \frac{U_0}{{I_{10}}^{H}{}_{\min} \cdot (L_{12} + L_{T12})} \cdot \frac{N}{f_s}\right) \end{aligned} \tag{42}$$

where $round(x)$ returns the nearest integrity smaller than x. The aim of choosing transient high-frequency energy within a specific frequency band of transient signal as a protection indicator is to obtain high robustness and reliability.

B. Threshold value determination

In this part, the thresholds are determined to judge whether an event is a fault or not. The classical method to find the correct threshold values is conducting multiple simulations through a systematic search. By concentrating on the worst-case situations, the threshold value can be defined in a relatively fast and straightforward manner. Considering the fault happens at the end of the Line 12, the DFT of fault current

component of Line 13 should be expressed as follows,

$$\begin{cases} I_{13}{}^{H}(s) = \dfrac{U_0}{s\cdot(sL_{T12}+1/sC_{c1})}\cdot h(s) \approx \dfrac{U_0}{s^2\cdot L_{T12}}\cdot h(s) \\ \left|X^{13}(k)\right| = \left|DFT(I_{13}(t))\right|_{\max} = \dfrac{N}{T}\cdot\left|\int_0^T L^{-1}(I_{13}{}^{H}(s))\cdot e^{-i\frac{2\pi}{T}kt}\cdot dt\right|_{s=k\cdot\frac{2\pi}{N}f_s\cdot j} \end{cases} \tag{43}$$

Accordingly, the transient high-frequency energy of Line 13 fault current can be approximately expressed as follows,

$$E^{13} = \frac{1}{N^2}\cdot\sum_{k=i}^{k=j}\left|X^{13}(k)\right|^2 \tag{44}$$

Therefore, the threshold value should be above the transient high-frequency energy of Line 13 fault current, when the fault happens at the beginning of the Line 12,

$$E^{set} = m\cdot E^{13} \tag{45}$$

where m is the concerned coefficient and is set above 1. In this paper, it is set as 1.2. The overall flow chart of the primary protection can be shown as Fig. 5. The transient high-frequency energy of the fault current within the specific frequency band can be referred as (41) and the primary protection scheme is triggered if the following equation is satisfied,

$$E > E^{set} \tag{46}$$

It should be pointed out that the length of the sampling window T and the fault detection time required are two different concepts. Actually, the fault detection time is far-less than the sampling window T since the sampling window T is rolling-time based. When the calculated transient energy of fault DC line current is above the set threshold, the DC fault will be detected immediately, normally less than 1ms.

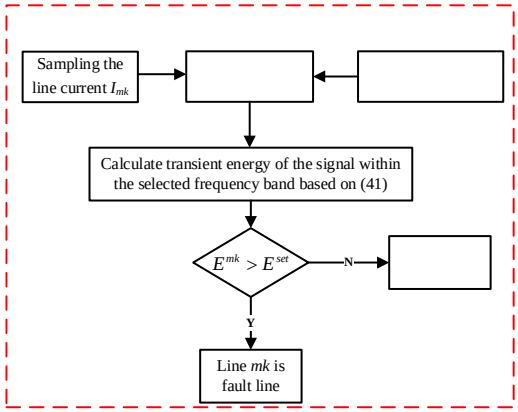

Fig. 5. The overall flow chart of the primary protection schemes for MTDC system.

C. *Sensitivity Analysis of proposed protection scheme*

Considering the fault happens at the end of the line 12 (the longest transmission line of MTDC system), the minimal fault current component can be indicated by (32). Combined (32) and (43), the ratio of high-frequency minimal fault current component at Line 12 and the maximal fault current component at Line 13 can be illustrated as follows,

$$\begin{aligned} \frac{\left|I_{12}{}^{H}(s)\right|_{\min}}{\left|I_{13}{}^{H}(s)\right|_{\max}} &\approx \left|\frac{L_{T12}}{L_{T12}+L_{12}}\cdot\frac{1}{h(s)}\right| = \left|\frac{L_{T12}/l}{L_{T12}/l+L_0}\cdot\frac{1}{h(s)}\right| \\ &= \left|\frac{z}{z+L_0}\cdot\frac{1}{h(s)}\right| \end{aligned} \tag{47}$$

where z is the correlated proportional coefficient, and it is defined as supplementary inductance L_{T12} divided by the length of the transmission line l. L_0 is the line inductance per-meter. It can be drawn from (47) that when the transmission line is long and the supplement inductance of L_{T12} is low, the coefficient z will be small, and the sensitivity of the protection scheme will be dramatically decreased. For a 500 km transmission line with 40 mH terminal inductance, combining (30), the Equation (47) becomes as follows,

$$\left.\frac{\left|I_{12}{}^{H}(s)\right|_{\min}}{\left|I_{13}{}^{H}(s)\right|_{\max}}\right|_{s=20\cdot\pi\cdot f_0\cdot j} \geq \left|\frac{25}{h(s)}\right| \geq \left|\frac{25}{99\cdot(2+k)}\right| \tag{48}$$

It is clearly indicated that the ratio of high-frequency fault current component of the faulted line and the healthy line is larger than 8 at the cut-off frequency of $10f_{oc}$ in the worst case situation. Actually, the capacitor of VSC C_{c1} has an impact on the sensitivity of the proposed protection scheme by influencing the cut-off frequency defined as (29). The smaller of the VSC capacitor, the larger of the cut-off frequency should be required for making sure low magnitude of $h(s)$ at the cut-off frequency. In order to increase the sensitivity of the protection scheme, higher cut-off frequency should be selected, and the lower threshold value is obtained for the protection scheme.

IV. The Influence of Traveling-wave on the Proposed Protection Scheme during Transient Process

When analyzing the transient process of MTDC grid during initial period after fault, the distributed parameter model of DC lines should be utilized. Transient current traveling-wave appears in the fault DC line, which impedes above analytical method based on the lumped parameter model. When the fault happens in the meshed MTDC, it can be regarded as a square-wave pulse generated from fault location and travelling among the entire system. Base on the Peterson's law [20], the first injection of current travelling wave is expressed as follows,

$$I_{12t,1} = \frac{2U_0}{Z_l} - \frac{2U_0}{Z_l}\cdot e^{-t/\tau_2} \tag{49}$$

where, Z_l is the wave impedance of current travelling wave, and it is normally as 400-500Ω. τ_2 is the time constant of current travelling wave, and can be expressed as follows,

$$\tau_2 = \frac{L_{T12}}{Z_l} \tag{50}$$

τ_2 is around 0.2ms when L_{T2} is selected as 100mH. When the fault happens at the end of the long transmission line, the transient process of first injection current travelling wave is finished, and the magnitude-frequency relationship of first injection current travelling wave $I_{12t,1}$ is expressed as follows,

$$\left|I_{12t,1}(\omega)\right| = \frac{2U_0}{T\cdot Z_l}\cdot\frac{1}{\sqrt{\omega^2+1/\tau_2{}^2}} \tag{51}$$

The sampling time T should be larger than the time when the next injection of current travelling wave comes at the beginning of the longest transmission line,

$$T \geq \frac{2l}{v} \tag{52}$$

where, v is the speed of travelling wave, which equals to $(L_0C_0)^{1/2}$. The inequality indicated by (52) guarantees the two line models (distributed parameter line model and lumped parameter line model) can be fairly compared during one injection travelling wave cycle. Combined (51) and (52), (51) is rewritten as follows,

$$\left|I_{12t,1}(\omega)\right| = \frac{U_0}{l \cdot L_0} \cdot \frac{1}{\sqrt{\omega^2 + 1/\tau_2^{\,2}}} \tag{53}$$

where, L_0 is the line inductance per-meter. Based on (35), when using the lumped parameter model of DC line, the magnitude-frequency relationship of transient DC fault line current I_{12L}, can be expressed as follows,

$$\left|I_{12L}(\omega)\right| = \frac{U_0}{\omega} \cdot \frac{1}{(L_0 + \frac{L_{T2}}{l})l} \tag{54}$$

Therefore, the ratio of frequency spectrum of transient fault line current with different line models is shown as follows,

$$\frac{\left|I_{12L}(\omega)\right|}{\left|I_{12t,1}(\omega)\right|} = \frac{L_0\sqrt{\omega^2 + 1/\tau_2^{\,2}}}{\omega(L_0 + \frac{L_{T2}}{l})} \approx \frac{L_0}{L_0 + \frac{L_{T2}}{l}} \tag{55}$$

For the health DC line, there is little traveling-wave effect when undergoing a DC fault in a meshed MTDC grid, so the fault component of healthy DC line with two line models (distributed line model and lumped parameter line model) are nearly the same. For the fault DC line, the error evaluation of the proposed high-frequency equivalent model and distributed line model during one reflection time cycle of current travelling wave can be indicated by (55). The ratio is around 0.83 for a 300 km DC line, which can be regarded as an acceptable range. If larger time window T is selected, the travelling wave effects are dramatically mitigated due to the several injections and reflections of travelling wave, and fault current with two line models are nearly the same. Even though the difference between two line models is relatively large when smaller time window T is selected (within first injection current travelling-wave), transient high-frequency energy of fault line with distributed line model will be larger than that with *RL* model, which is clearly indicated by (51). Therefore, setting high ratio of transient high-frequency energy of fault line and healthy line current based on high-frequency equivalent model guarantees the accuracy and sensitivity of the proposed primary protection scheme.

V. Further Discussion of Three Different Models Involved

When analyzing the transient process of MTDC grid during DC fault for a long transmission line, transient current travelling-wave will appear in the fault DC line. Existing rate of change of current or voltage (ROCOC or ROCOV) method and travelling-wave method are mainly based on the first reflection of the travelling wave at the inductive termination of lines, which can be well mathematically expressed based on Peterson's law. For the successive reflections of the travelling wave, the mathematical expressions cannot be easily obtained, and the fault characteristics based on the distributed line model cannot be clearly expressed. Therefore, the existing methods require extremely high-sampling frequency (hundreds of kHz or 1MHz) so that the first reflection of the current/voltage travelling-wave can be captured. In addition, the rate of change of current or the voltage dramatically decays with the time. Normally, in the practical engineering, the primary protection relay will be activated by detecting three or four continuous ROCOC or ROCOV that are over the set threshold. As a result, the primary protection based on ROCOC or traveling-wave methods is vulnerably invalid when the sampling frequency is relatively low, or missing the first few data of initial DC fault current.

When analyzing one meshed and complex network, the classical model is the lumped parameter models (*RL* models). The two line models (distributed line model and lumped parameter line model) are basically the same, when the transmission line is short or the travelling-wave effects are dramatically mitigated with the time passing by. Even though the classical *RL* based model is fully discussed and easily solved by classical *Laplace Transformation* or the *State Space* method, it can not provide the clear analytical expressions of the fault current nor the parameters that influence the fault current when the network is large and complicated.

Therefore, a high-frequency equivalent model of VSC based MTDC system is firstly proposed for the initial DC fault current calculation. In the proposed model, the low-frequency part of the DC fault current is overlooked, and the initial fault current calculation of the fault DC line and the healthy DC line can be reduced as two simplified *RLC* circuits as shown in Fig. 4. The proposed high-frequency equivalent model has relatively high-accuracy compared to the *RL* models of lines in terms of the initial DC fault current calculation. The main advantage of the proposed high-frequency equivalent model is to give a clear analytical expression of the initial fault DC current for a large and complex meshed grid, which can be utilized for systematically primary protection design and threshold setting.

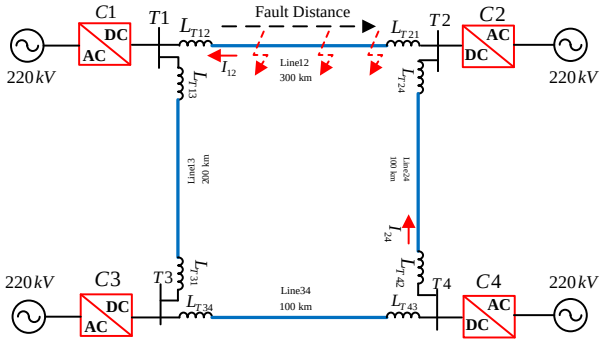

Fig. 6. The outline of the four-terminal DC grid

VI. Simulation Studies

In order to validate the effectiveness of the proposed protection scheme, a four-terminal HVDC grid [19] modeled in PSCAD/EMTDC is shown in Fig. 6. The DC reactors of 100 mH are implemented at each end of DC overhead lines. The

capacitance of VSC capacitor and the short circuit ratios (SCR) of equivalent AC systems are provided in Table I. Each VSC with detailed switching model is connected through DC lines of frequency dependent representation. Converter station *C*1, *C*3, and *C*4 are in active and reactive control model [21], while the converter station *C*2 controls DC-link voltage and the exchanged reactive power with connected ac grid.

A. Model verification and threshold calculation

In the lumped parameter model, the correlated coefficient τ can be calculated based on (27). Considering the fault happens at the end of the Line 12, the proportional coefficient of Line 13 and Line 24 current (k) reaches maximal and can be calculated based on (5). Correspondingly, the paralleled resonance frequency of Line 24 and DC-link capacitor of C_{c2}, marked as f_{oc} is obtained based on (28) shown in Table I. In order to eliminate the influence of high-frequency steady-state harmonics and noises, the magnitude of minimal detectable current $I_{10}{}^{H}{}_{\min}$ is set as 10 A in the paper. Therefore, the range of the cut-off frequency f_{cut} is formulated based on (37). The sampling frequency f_s is selected as 50 kHz in the paper. The time window T should cover the time interval of two continuous injections of current traveling-wave in the longest transmission line, and the sampling number N is selected as 128 for facilitating calculating the FFT of signal. The range of selected frequency band number (i, j) can be referred as (42). The threshold value for the protection scheme E_{set} is calculated based on the transient high-frequency energy of Line 24 current considering the fault happens at the end of Line 12.

TABLE I PARAMETERS OF TEST MTDC SYSTEM

Symbol	Item	Value
C_{ci}	Capacitor of VSC	800 μF
L_{Tij}	Supplementary Inductance	100 mH
L_0	Inductance per kilometer of DC line	1.634 mH
τ	Defined correlated coefficient	0.290 ms
f_{oc}	Resonance frequency of DC line	34.9Hz
$I_{10}{}^{H}{}_{\min}$	Magnitude of minimal detectable current	10 A
f_{cut}	Range of cut off frequency	349~5394 Hz
f_s	Sampling frequency	50 kHz
N	Sampling number in a cycle	128
T	Time Window in a cycle	2.56 ms
(i,j)	The range of selected frequency band	(1,13)
E_{set}	Threshold value	8.4E-5

Fig. 7 shows the simulation results when the metallic fault happens at the end of Line 12. Three different models with lumped parameter of DC line (RL model), with frequency dependent (FD) model of DC line, and with proposed high-frequency (HF) equivalent model are compared in Fig. 7. It is clearly seen from Fig. 7 (a) that with FD model, the travelling wave effects appear in Line 12, and the fault current begins to surge when the first injection of current travelling-wave comes at L_{T12}, located at the beginning of Line 12 at t=1.001s. With RL model, the fault current curve that increases smoothly at t=1s is very similar to that with HF model. It is well verified that when analyzing transient process during initial period after fault, the complex circuit network can be simplified as high-frequency model of original network with high-accuracy. With RL model and HF model, the transient high-frequency energy of Line 12 current is nearly the same as 0.03 shown in Fig. 7 (b). However, the transient high-frequency energy of Line 12 current with detailed FD model is smaller than that with RL or HF model since there is a slightly DC current increase when the next injection of current travelling wave comes, as shown in Fig. 7 (a). Fig. 7 (c) and (d) indicate that there is no traveling-wave in the healthy line (Line 24), which results in line current curve and the magnitude of FFT of line current very similar based on three different line models. The transient high-frequency energy of healthy line current in the worst condition is calculated as 7.0e-5 based on HF model. Accordingly, the threshold value for the primary protection scheme E_{set} is set as 8.4e-5 as shown in Table I.

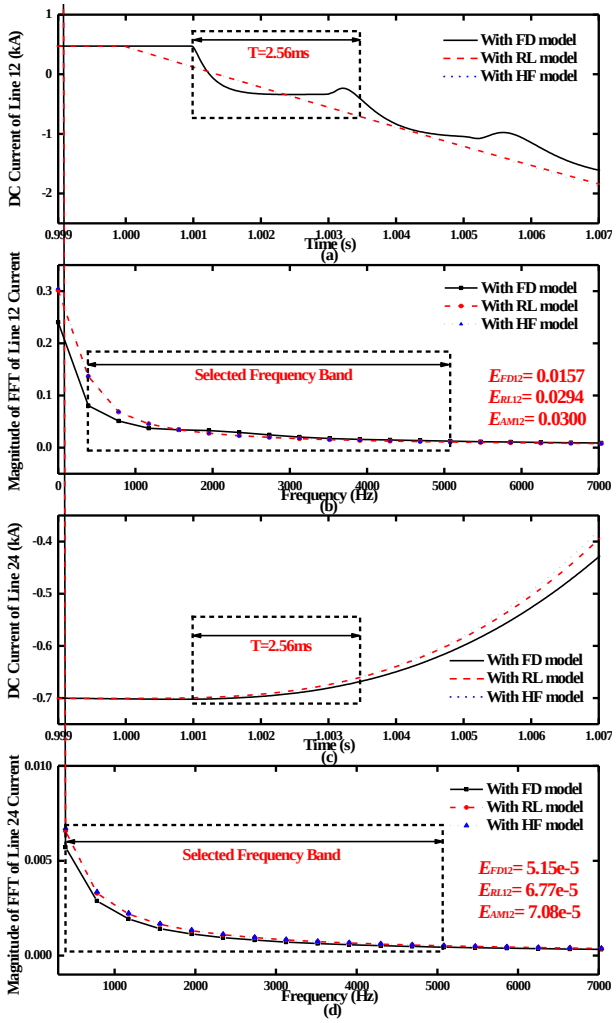

Fig. 7. Simulation Results with different models.

B. Influence of time window and fault location

Table II shows the impact of different selected time windows on the transient high-frequency energy of fault DC line current with different models involved when the fault happens at the end of Line 12. Table II shows that when time window T less than 2 *ms*, the transient high-frequency energy of fault DC line current with FD model is higher than that with RL and HF model, since the rate of change of fault current with FD model is higher than that with the other two models. However, the transient high-frequency energy of fault DC line current with FD model is smaller than that with RL and HF model when larger time window is selected. This can be explained by the fact that the fault DC current with FD model undergoes a

slightly increase when the second injection of current travelling wave comes at the beginning of Line 12. The ratio of transient high-frequency energy of fault line current with FD model and HF model as shown in Table III is 1.91. The difference between transient high-frequency energy of fault line current with RL model and HF model is small with different time windows, and it is well verified the proposed HF model can be applied for analyzing transient fault current during initial short period.

TABLE II INFLUENCE OF TIME WINDOWS ON PROPOSED PROTECTION SCHEME

	T=1 ms	T=2 ms	T=2.26ms	T=2.56 ms
With FD model	0.0176	0.012	0.0139	0.0157
With RL model	0.005	0.011	0.0180	0.0294
With HF model	0.0054	0.0112	0.0183	0.0300
Ratio of Energy Using HF and using FD	0.284	0.993	1.32	1.91

Table III shows the transient high-frequency energy of fault line and healthy line current with different fault locations. It is clearly seen that the transient high-frequency energy of fault line current increases with the decrease of the fault locations. In addition, the ratio of transient high-frequency energy of fault line current with FD model and HF model is decreasing with the decrease of the fault locations. This can be explained by the fact that the travelling wave on the fault line decays dramatically in several injections and reflections. Therefore, using RL or HF model can reflect the dynamics of the system during fault with the decrease of the fault locations. With the decrease of the fault locations, the transient high-frequency energy of healthy DC line current decreases quickly as shown in Table III. The ratio of transient high-frequency energy of fault line and healthy line current is above 400, which verifies the high-sensitivity of primary protection scheme.

TABLE III INFLUENCE OF FAULT LOCATIONS ON THE PROTECTION SCHEME

Fault Location (km)	Transient high-frequency energy of fault line (Line 12)			
	FD model	RL model	HF	Ratio
300	0.0157	0.0297	0.0300	1.91
250	0.0221	0.0403	0.0410	1.85
200	0.0435	0.0565	0.0576	1.32
150	0.0648	0.0868	0.0882	1.36
100	0.1157	0.1491	0.1515	1.31
50	0.2524	0.3100	0.3180	1.25
Fault Location (km)	Transient high-frequency energy of healthy line (Line 24)			
	With FD model	With RL model	With HF	
300	5.15E-05	6.77E-05	7.08E-05	
250	1.12E-05	1.49E-05	1.69E-05	
200	3.03E-06	4.56E-06	5.93E-06	
150	9.31E-07	2.78E-06	3.47E-06	
100	3.96E-07	7.15E-07	1.01E-06	
50	1.67E-07	4.37E-07	5.82E-07	

Fig. 8 shows the fault current component of Line 12 and Line 24 when the metallic fault happens at 100 km and 200 km away from the beginning of the Line 12. Fig. 8 (a) shows the change of fault current component of Line 12 with FD model and with RL model are nearly the same within the selected time windows. Therefore, RL model of DC line can be utilized for fault current analysis with an acceptable error. In addition, it shows that high-frequency equivalent model has high-accuracy compared to RL model within short-time period, as illustrated in Fig. 8 (a) and (c). As shown in Fig. 8 (b), the magnitude of FFT of fault current component of Line 12 has high value at the frequency of 790 Hz with fault location of 100 km and at the frequency of 1170 Hz with fault location of 200 km, which explains the travelling wave injects and reflects back and forth on the fault DC line. With the decrease of fault locations, the fault current component of Line 12 surges increasingly and the fault current component of Line 24 decreases dramatically.

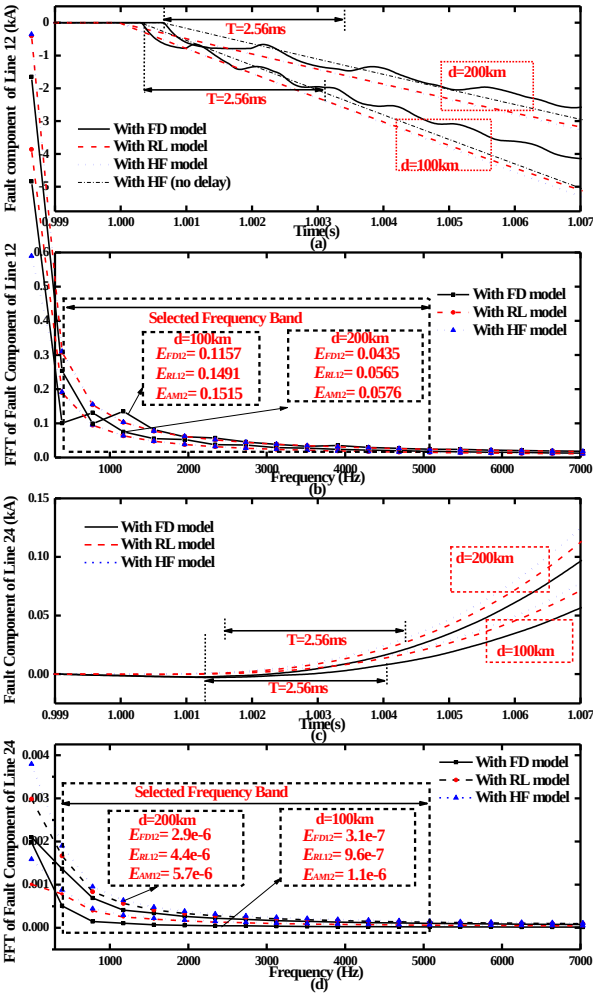

Fig. 8 Simulation Results with different models under different fault locations.

C. *Influence of fault resistance*

Table IV compares the transient high-frequency energy of fault line current under different fault resistance with different models. It can be clearly seen that with the increase of the fault resistance, the transient high-frequency energy of Line 12 current is decreasing. As shown in Fig. 9, with high fault resistance at the end of Line 12, the fault current component with FD model has apparent oscillation. This characteristic makes the transient high-frequency energy of Line 12 current has high-value with FD model compared that with the other two models shown in Table IV. Therefore, the proposed protection scheme that utilizes the transient high-frequency energy of line current has high-sensitivity when the current travelling-wave exists. As shown in Fig. 9 (a) and (c), the fault component of Line 12 with FD model and RL model are gradually the same in the long simulation time since the current travelling-wave with FD model will gradually decay after several injections and reflections. The transient high-frequency energy of the fault line with RL model and the proposed HF model is nearly the same under different fault resistances. It can be concluded that

during initial short period after fault, the proposed HF model can be utilized for fault analysis. With HF model, the transient high-frequency energy of Line 12 current is 1.61e-4 under 300 Ω fault resistance, which is larger than the threshold set as 8.4e-5. Simulation results show that the proposed protection scheme can tolerant 1.5 p.u. fault resistance.

TABLE IV INFLUENCE OF FAULT RESISTANCES ON PROPOSED SCHEME

Fault Location (d=300 km)	Transient high-frequency energy of Line 12 current		
	100 Ω (0.5 p.u.)	200 Ω (1 p.u.)	300 Ω (1.5 p.u.)
FD model	0.0072	0.0056	0.004
RL model	0.0025	5.02E-4	1.63E-4
HF model	0.0025	4.98E-4	1.61E-4
Fault Location (d=200 km)	Transient high-frequency energy of Line 12 current		
	100 Ω (0.5 p.u.)	200 Ω (1 p.u.)	300 Ω (1.5 p.u.)
FD model	0.0081	0.0041	0.0029
RL model	0.0135	0.0043	0.0017
HF model	0.0136	0.0043	0.0017

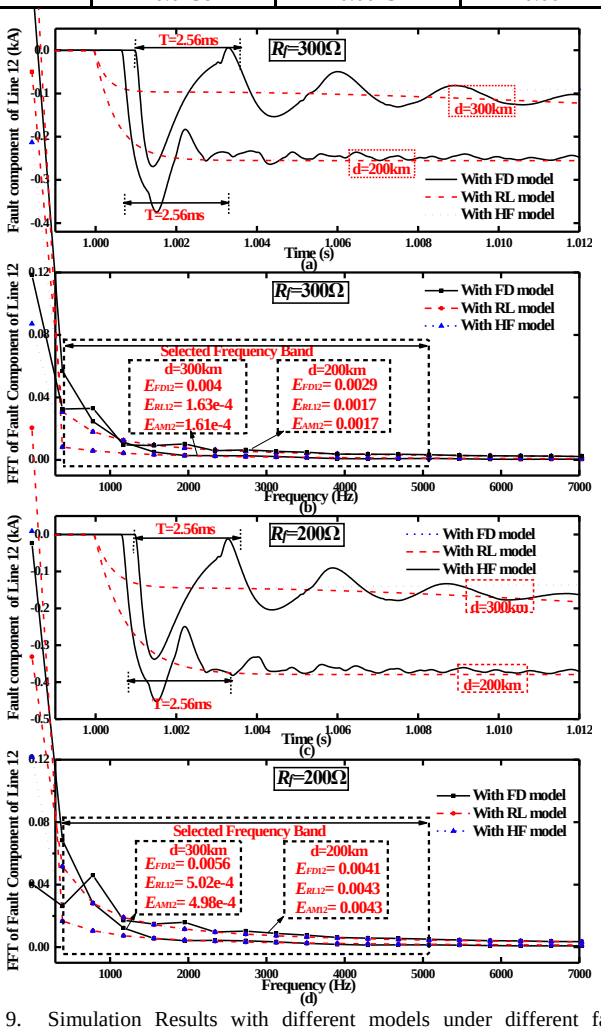

Fig. 9. Simulation Results with different models under different fault resistances at different fault locations.

D. Comparison with the ROCOC based protection schemes

Fig.10 compares the performance of different DC fault detection methods (proposed transient high-frequency energy of current and rate of change of current (ROCOC) method) with relatively low sampling frequency at 5 kHz under different fault resistances. With metallic fault, the rate of change of Line 12 current has high value when the first injection of current traveling wave arrives at the inductance terminal at t=1.001s, which verifies the high-sensitivity of the ROCOC method for DC fault detection. However, the ROCOC value decreases dramatically with the time. It can be clearly seen that the fourth and fifth ROCOC value comes to -0.24 and -0.1 as shown in Fig. 10 (a), which is vulnerably below the set threshold. In addition, when the sampling frequency is further decreasing, or missing the first few data of initial DC fault current, the primary protection based on ROCOC becomes invalid. However, the proposed DC fault detection method based on transient high-frequency energy of current does not depend on the high sampling frequency. The transient high-frequency energy of Line 12 reaches to 0.0130 with 5 kHz sampling frequency, which is almost the same as the value (0.012) with 50kHz sampling frequency. With 300 Ω fault resistance, the transient travelling-wave fast decays as shown in Fig. 10 (c). The difference between third and fifth sampling point of fault component of Line 12 is very small, which might result in the primary protection based on ROCOC invalid. However, the transient high-frequency energy of Line 12 with 5 kHz sampling frequency is almost the same as that with 50kHz sampling frequency as shown in Fig. 10 (d), which verifies the high robustness of the proposed protection scheme.

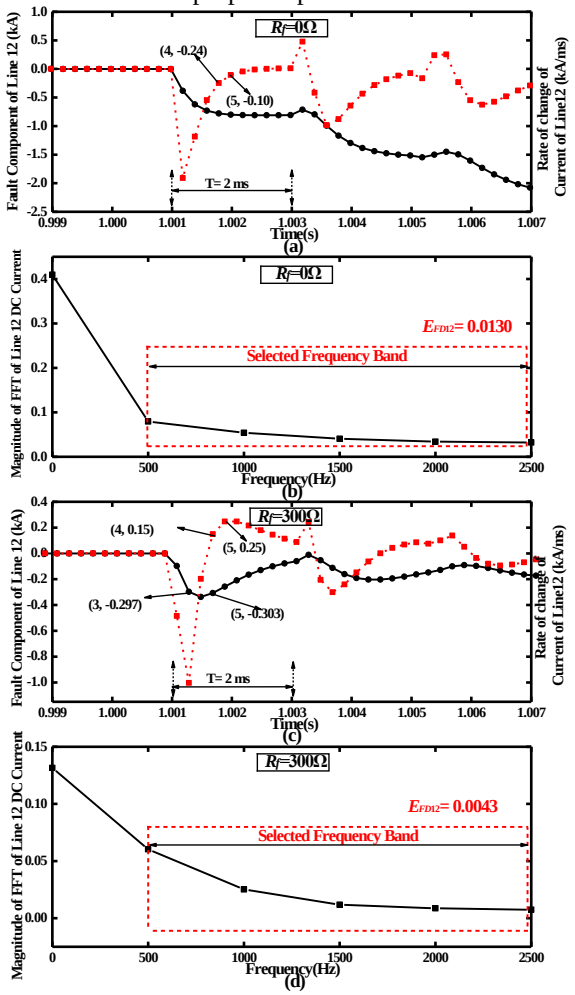

Fig. 10. Simulation results with different protection schemes under different fault resistances.

E. Impact of component parameters and outside noises

Fig. 11 shows the impact of component parameters and outside noises on the proposed protection scheme. Fig. 11 (a)

and (b) shows the simulation results with the metallic fault happening at the end of the long transmission line of 500 km. When smaller supplementary inductance L_{T12} (40 mH) is selected, the fault component of Line 12 increases faster than that with larger L_{T12} implemented. The transient high-frequency energy of Line 12 current with FD model is calculated as 0.0124 when the time window T is selected as 2.56 ms. This value is nearly the same as the transient high-frequency energy of Line 12 current with fault at the end of transmission line of 300 km. However, the transient high-frequency energy of Line 24 (health line) increases largely with the decrease of the supplementary inductance L_{T12}, which can be clearly seen from (43). With the fault happens at the end of transmission line of 500 km and L_{T12} of 40 mH, the ratio of transient high-frequency energy of fault line and healthy line current is nearly 20, which guarantees the high-sensitivity of primary protection scheme. Fig. 11 (c) and (d) shows the noises-robustness tests on the proposed protection scheme. The added outside noise is Gaussian noise with a signal-to-noise ratio (SNR) of 32, which can be seen from Fig. 11 (c). The transient high-frequency energy of Line 12 with outside noises is the similar to that without noises as shown in Fig. 11 (d), which indicates that the proposed protection scheme has high-robustness to the outside noises.

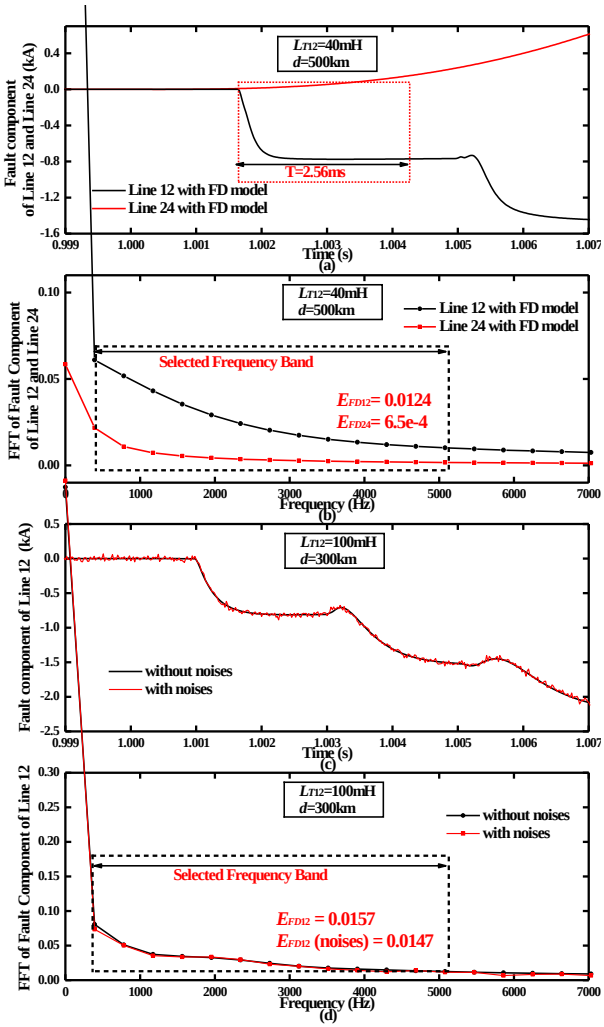

Fig. 11 Impact of component parameters and outside noises on the proposed protection scheme.

VII. Conclusion

This paper firstly proposes a high-frequency equivalent model of VSC-MTDC system for fault current calculation during initial short period after fault. Accordingly, a novel DC fault detection method for VSC based MTDC system that utilizes the transient high-frequency energy of line current is further proposed. In the scheme, the fault line can be identified fast with one-end signal. In addition, the influence of transient travelling-wave on the proposed protection scheme is also investigated. It is concluded that the transient travelling wave on the fault line has very limited impact on the accurate operation of proposed primary protection. Numerous simulation studies have demonstrated that the proposed high-frequency equivalent model can be utilized for fault analysis of MTDC system and the proposed scheme is effective in different time windows, different fault locations and high fault resistances. Compared with the traditional protection schemes based on ROCOC, the proposed one stands out for relatively low sampling frequency, insensitive to the parameter changes, and high robustness with respect to the outside noises and data missing.

References

[1] R. Shah, J. C. Sánchez, R. Preece and M. Barnes, "Stability and control of mixed AC–DC systems with VSC-HVDC: a review," *IET Generation, Transmission & Distribution*, vol. 12, no. 10, pp. 2207-2219, 5 29 2018.

[2] Y. Li, Z. Xu, J. Østergaard and D. J. Hill, "Coordinated Control Strategies for Offshore Wind Farm Integration via VSC-HVDC for System Frequency Support," *IEEE Transactions on Energy Conversion*, vol. 32, no. 3, pp. 843-856, Sept. 2017.

[3] MacIlwain C. Energy: supergrid. Nature 2010;468(7324):624–5.

[4] P. Han and S. Wang, "Parameter coordination of modular multilevel converter for robust design during DC pole to pole fault," *Proc. China Int. Conf. Elect. Distrib*., 2012, pp. 1–5.

[5] G. Zhang, Y. Chen, C. Yue, L. Qi, and J. Pan, "DC pole-to-pole short circuit behavior analysis of modular multilevel converter," *Proc. 2014 IEEE Energy Convers. Congr. Expo*., 2014, pp. 5698–5702.

[6] J. Rafferty, L. Xu, and D. J. Morrow, "DC fault analysis of VSC based multi-terminal HVDC systems, " *Proc. IET Int. Conf. AC DC Power Transmiss*., Birmingham, U.K., 2012, pp. 1–6.

[7] Z. Zhang and Z. Xu, "Short-circuit current calculation and performance requirement of HVDC breakers for MMC-MTDC systems, " *IEEJ Trans. Elect. Electron. Eng*., vol. 11, no. 2, pp. 168–177, Mar. 2016.

[8] C. Li, C. Zhao, J. Xu, Y. Ji, F. Zhang and T. An, "A Pole-to-Pole Short-Circuit Fault Current Calculation Method for DC Grids," *IEEE Transactions on Power Systems*, vol. 32, no. 6, pp. 4943-4953, Nov. 2017.

[9] J. Descloux, P. Rault, S. Nguefeu, J. B. Curis, X. Guillaud, F. Colas, et al., "HVDC meshed grid: Control and protection of a multi-terminal HVDC system," CIGRE, 2012.

[10] J. Sneath and A. D. Rajapakse, "Fault Detection and Interruption in an Earthed HVDC Grid Using ROCOV and Hybrid DC Breakers," *IEEE Transactions on Power Delivery*, vol. 31, no. 3, pp. 973-981, June 2016.

[11] Z. Zheng, T. Tai, J. S. Thorp and Y. Yang, "A Transient Harmonic Current Protection Scheme for HVDC Transmission Line," *IEEE Transactions on Power Delivery*, vol. 27, no. 4, pp. 2278-2285, Oct. 2012.

[12] J. Liu, N. Tai, C. Fan and W. Huang, "Protection scheme for high-voltage direct-current transmission lines based on transient AC current," *IET Generation, Transmission & Distribution*, vol. 9, no. 16, pp. 2633-2643, 12 3 2015.

[13] F. Kong, Z. Hao, S. Zhang, and B. Zhang, "Development of a novel protection device for bipolar HVDC transmission lines," *IEEE Transactions on Power Delivery*., vol. 29, no. 5, pp. 2270–2278, Oct. 2014.

[14] W. Leterme, J. Beerten, and D.VanHertem, "Nonunit protection of HVDC grids with inductive DC cable termination," *IEEE Transactions on Power Delivery*., vol. 31, no. 2, pp. 820–828, Apr. 2016.

[15] J. Beerten, S. Cole, and R. Belmans, "Modeling of Multi-Terminal VSC HVDC Systems With Distributed DC Voltage Control," *IEEE Transactions on Power Systems*, vol. 29, pp. 34-42, Jan 2014.
[16] R. Li; L. Xu; L. Yao, "DC Fault Detection and Location in Meshed Multi-terminal HVDC Systems Based on DC Reactor Voltage Change Rate," *IEEE Transactions on Power Delivery*., vol.32, no.3, pp. 1516-1526, June 2017.
[17] C. Li, A. M. Gole and C. Zhao, "A Fast DC Fault Detection Method Using DC Reactor Voltages in HVDC Grids," *IEEE Transactions on Power Delivery*. to be published.
[18] J. Liu, N. Tai and C. Fan, "Transient-Voltage-Based Protection Scheme for DC Line Faults in the Multiterminal VSC-HVDC System," *IEEE Transactions on Power Delivery*, vol. 32, no. 3, pp. 1483-1494, June 2017.
[19] J. Beerten and R. Belmans, "Analysis of Power Sharing and Voltage Deviations in Droop-Controlled DC Grids," *IEEE Transactions on Power Systems*, vol. 28, no. 4, pp. 4588-4597, Nov. 2013.
[20] L. V. Bewley, "Traveling Waves on Transmission Systems," *Transactions of the American Institute of Electrical Engineers*, vol. 50, no. 2, pp. 532–550, Jun. 1931.
[21] L. Xu, L. Z. Yao, and C. Sasse, "Grid integration of large DFIG-based wind farms using VSC transmission," *IEEE Transactions on Power Systems*, vol. 22, pp. 976-984, Aug 2007.

Yujun Li received his B.Sc and M.Sc degrees from Xi'an Jiaotong University, China, in 2011, and Zhejiang University, China, in 2014 in Electrical Engineering, respectively. He received the Ph.D degree in Hong Kong Polytechnic University in 2017. From 2017 to now, he is a lecturer in Xi'an Jiaotong University, China. His main fields of interest include grid integration of renewable energy and HVDC modeling.

Lei Wu received his B.Sc degree from Nanjing Institute of Technology, China, in 2017.He is currently pursuing the M.Sc degree in Xi'an Jiaotong University, China. His research interest include protective relaying and VSC-HVDC.

Jiapeng Li received the B.Eng. degree in electrical engineering from Xi'an Jiaotong University, Xi'an, China, in 2017, and is currently pursuing the M.E. degree at Xi'an Jiaotong University. His research interests include protection and fault location of HVDC system.

Liansong Xiong (S'13-M'16) received his B.S., M.S. and Ph.D. degrees in Electrical Engineering from Xi'an Jiaotong University, Xi'an, China, in 2009, 2012 and 2016, respectively. In June 2016, he joined the School of Automation, Nanjing Institute of Technology (NJIT), introduced in "High-Level Academic Talent Plan of NJIT". His current research interests include power quality, multi-level converter, renewable energy generation, micro-grids, and stability analysis of grid-tied inverter dominated power systems.

Guobing Song (M'10) received the PH.D degree in electrical engineering at the Xi'an Jiaotong University, Xi'an, China, in 2005. Currently he works in the Xi'an Jiaotong University. His research interests include transmission line fault location and protections.

Zhao Xu (M'06–SM'13) received the Ph.D. degree in electrical engineering from The University of Queensland, Brisbane, Australia, in 2006.From 2006 to 2009, he was an Assistant and later Associate Professor with the Centre for Electric Technology, Technical University of Denmark, Lyngby, Denmark. Since 2010, he has been with Hong Kong Polytechnic University. His research interests include demand side, grid integration of wind power, electricity market planning and management, and AI applications. He is an Editor of the Electric Power Components and Systems journal.